A Prototype Vision System for Analyzing CT Imagery of Hardwood Logs

Dongping Zhu, *Member, IEEE*, Richard W. Conners, *Member, IEEE*, Daniel L. Schmoldt, and Philip A. Araman

Abstract— To fully optimize the value of material produced from a hardwood log requires information about type and location of internal defects in the log. This paper describes a prototype vision system that automatically locates and identifies certain classes of defects in hardwood logs. This system uses computer tomograph (CT) imagery. The system uses a number of processing steps. First, an adaptive filter smoothes each 2-Dimensional CT image to eliminate annual ring structure while preserving other image details. Second, a multi-threshold 2-D segmentation scheme is used to separate potential defect areas from areas of clear wood on each CT image. This differentiation is based on density variations and the fact that most of the log is clear wood. Third, by generalizing 8-neighbor connectivity to 3-dimensions, sequences of consecutive, segmented 2-D slices are then analyzed to find connected 3-D regions. Because of the natural variability of wood and the variety of ways defects manifest themselves in logs, there is considerable imprecision and ambiguity in assigning labels to these 3-D regions. One consequence of this variability is that exact 3-D geometric models seemingly cannot be used in the recognition process. Therefore, a set of basic features are defined to capture basic 3-D characteristics of wood defects. For 3-D object (defect) recognition, a set of hypothesis tests are employed that use this set of features. To further help cope with the above mentioned variability, the Dempster-Shafer theory of evidential reasoning is used to classify defect objects. Results of preliminary experiments employing two very different types of hardwood logs are given. The logs used are southern red oak, a group of ring porous species, and yellow poplar, a diffuse porous species. These two log types represent the two extremes in hardwood anatomy. Initial experimental results demonstrate the feasibility of the proposed vision system.

I. INTRODUCTION

STEADILY increasing costs of raw materials and labor in the manufacture of lumber and veneer demand improved methods for processing wood. Because the costs of logs can constitute up to 75% of the production cost in US sawmills, optimizing wood conversion into useful products is an economic necessity [6], [17], [33], [38], [42]. Automated log inspection systems can potentially increase mill productivity and improve the quality of the material derived from logs. The value of

D. Zhu was with the Spatial Data Analysis Laboratory, The Bradley Department of Electrical Engineering, Virginia Polytechnic Institute and State University, Blacksburg, VA 24061 USA. He is now with Globalstar, L. P. San Jose, CA 95164-0670 USA (e-mail: dpz@gstar2.globalstar.loral.com).

R. W. Conners is with The Bradley Department of Electrical Engineering, Virginia Polytechnic Institute and State University, Blacksburg, VA 24061-0111 USA.

D. L. Schmoldt and P. A. Araman are with the USDA Forest Service, Southeastern Forest Experiment Station, Virginia Polytechnic Institute and State University, Blacksburg, VA 24061-0503 USA.

Publisher Item Identifier S 1083-4419(96)03924-6.

hardwood lumber cut from a log depends on the lumber's quality which in turn depends on the size and number of clear areas on a board's surface. It therefore seems reasonable to suppose that if one can locate and identify the internal defects in a log prior to its breakdowninto lumber, one should be able to formulate a method for cutting the log into lumber that has the highest possible value.

A defect in wood is any feature that lowers its market value; wood defects, such as knots, holes, stains, and decay, all affect the grade of lumber. The fewer defects a piece of lumber has, the higher is its grade. Numerous studies suggest that at least 10 to 21% improvement in lumber value can result from a well-chosen breakdown strategy [22], [27], [33]. Currently, log inspection is performed by human experts, but their performance is quite limited. Selecting the best log breakdown strategy is a difficult task that calls for the application of more quantitative methods. While the work in [11], [19] represents an important step toward this goal, no one has attempted to create a general-purpose machine vision system for the automated analysis of log images.

This work aims to demonstrate the feasibility of automatically inspecting hardwood logs for a subset of defects using a prototype vision system. Computer tomography (CT) enables one to detect a wide range of wood defects, including knots, splits, decays, bark, voids, holes, and etc. [1], [37], [40]. In this study, however, a limited number of wood defects, such as knots, decay, and bark, could be used, due to limited log data available. The prototype system consists of 3 components: (1) a data acquisition unit (e.g., CT scanner), (2) an image segmentation module, and (3) a scene analysis module. Nevertheless, the work described here does not address the collection of images, but focuses instead on computer interpretation of acquired CT images. Section II reviews related work on automated wood inspection. Section III describes the segmentation module and Section IV presents the scene analysis module. In Section V we offer some experimental results from the application of the prototype vision system. Finally, Section VI provides conclusions, and proposes future research directions.

II. PROBLEM BACKGROUND

A. Wood Image Analysis

In recent years, much research on hardwood timber processing has been focused on two closely related areas, optimal breakdown strategy and log scanning. To better utilize knowledge about internal defects in log scanning, some researchers have examined optimal breakdown strategies [27], [33]. Most

of the efforts to date have involved computer simulations to evaluate increased value recovery from optimized breakdown. Little has been done, however, to integrate optimal breakdown and internal imaging of logs by analyzing scanned images for optimal cut-up decisions.

While attempts are being made to find new and better sawing patterns, during the last 10 years some computer-aided sawing systems have been introduced into sawmills. Generally, these systems try to estimate the external shape of logs using data from a set of light beams and photo-sensors, or from a close circuit video camera. Because these systems can measure a log's shape more accurately than a human operator, to some extent they are able to improve *volume* yield. These systems, however, do not optimize value yield from logs, because value yield is closely tied to the location of defects on sawn products, which external scanning systems ignore.

Other log inspection techniques for measuring a log's shape have been tested. These include using ultrasound [2], laser [21], optical scanners [24], and microwave [26], and computed tomograph [1], [8], [12], [13], [15], [31], [32], [40]. For example, an optical scanner is used in [24] to obtain the profile of a log, and a parametric paraboloid function models the internal projection of knots. Based on this mathematical model, the location, shape, size, and orientation of knots are predicted. The information obtained is then used in knot-related grading rules so that an optimal log cutting pattern can be specified. In an experiment performed using 10 test logs, this system improved the value recovery by 7.5%.

Recent efforts to improve value recovery from sawlogs have used new technologies, such as CT and magnetic resonance imaging (MRI) to obtain 3-D information about the internal defects of sawlogs [37], [39]. An initial study of CT's feasibility for sawmill use evaluated its capability for detecting knots [35]. A more complete evaluation of CT's usefulness for identifying defects was reported in [11] where 3 features were derived from the images and were then used in a recognition process. These 3 features were: (1) pixel density, (2) object shape, and (3) growth ring texture patterns. In its decisionmaking stage, this vision system recognized knots by pixel density and 2-D shape, clear wood by the circular patterns of growth rings, decay by density and growth ring patterns, and image background by density. This system was able to successfully identify knots, decay, holes, and clear wood using CT-scans of sawlogs.

The work in [11] represents the first attempt to automatically classify internal wood structures by analyzing scanned data. Not surprisingly, this study has several limitations. First, it was not tested on log features other than those reported, e.g., bark and compression wood. Second, the methods were only tested on image samples from 3 softwood species. Hence, the robustness of the system for hardwoods has not been established. Third, no attempt was made to deal with the possible "noise" problem inherent in CT imaging. For example, the unwanted annual rings in log images, if not eliminated at an early stage, could misguide the identification task. Furthermore, because annual rings are present in most parts of a CT image, processing them will significantly reduce vision system throughput. Fourth, object identification was based on insufficient infor-

mation to apply to a generalized vision system because 3-D topological and geometric features were not utilized.

B. Knowledge-Based Vision in Wood Inspection

While no general method to automatically interpret log CT images currently exists, progress has been made toward machine vision systems for lumber inspection. A common feature of these vision systems is that they combine computed feature information with a reasoning process using either texture-related measures [7], decision trees [23], or knowledge-based systems [6], [42]. Successful application of machine vision systems to lumber quality inspection indicates that their methods might also be adopted to the log inspection problem if an appropriate imaging method is used.

Knowledge-based systems have been used successfully for machine vision system applications. There are normally two levels of information processing in industrial machine vision systems: image segmentation and image interpretation. Image segmentation separates regions of interest from the rest of the image, while image interpretation labels image regions by using both low-level information, i.e. transformed scan data, and high-level, domain specific knowledge (often in the form of heuristic production rules). Knowledge sources extract image feature information from a subset of regions in a segmented image, this can include spectral, texture, shape, and spatial attributes of regions. Based on image feature information, knowledge sources form opinions about the presence or absence of objects they are capable of observing. Belief about the identity of objects, based on these opinions, will be imperfect, however. At best, such opinions can only be viewed as evidence to suggest the presence or absence of semantically meaningful entities in a particular scene of interest.

To represent uncertainty in expert systems, inexact reasoning methods are often used. In many circumstances, a pure probabilistic-based approach to reasoning in complex domains is overly restrictive. As a consequence, probabilistic approaches are typically compromised by making ad hoc modifications to Bayes' rule [18]. The Dempster-Shafer (D-S) theory of evidence [9], [29], on the other hand, relaxes the principle of the excluded middle used in probability theory. In principle, it is a formal and uniform representation of ignorance, and it can distinguish disbelief from belief.

Evidential reasoning based on Dempster's rules [9] can be used to combine evidence about an object that is collected from different knowledge sources. It provides an intuitive method for reasoning under uncertainty because, in this theory, evidence that only partially favors a hypothesis is not construed as also partially supporting its negation. This means, belief in the negation of a hypothesis is treated independently from belief in the hypothesis. D-S has been successfully applied to uncertainty reasoning in knowledge-based machine vision systems [6], [16]. The benefit of employing such techniques is that a vision system is able to correctly label a significantly greater number of regions in an image, by using previously unavailable information such as the amount of ignorance or ambiguity that a label (classification) hypothesis exhibits. In the context of industrial vision system applications, this means that this method of inexact reasoning has the

potential to produce more accurate inspection in an automated environment.

Object recognition is the primary goal for many industrial vision systems. One key issue that plagues object recognition is dealing with the inherent uncertainty of data measurements from real devices and real scenes. Most current methods are suited to recognition tasks where objects have regular shapes or they can be approximated by mathematically described shapes, such as cylinders, spheres, or ellipsoids, or by physical and anatomical models. In many real-world circumstances, however, a recognition procedure must deal with objects having complex shapes, for which exact geometric models are difficult to obtain. Some authors [34] argue that contextual information is central to solving it. Generally, information content in 3-D is considerably richer than that in 2-D. Because the 3-D shape of anatomic structures in a log may contain correspondingly large amounts of information useful for eventual log sawing, it is advantageous to explore methods for extraction and classification of information directly from the 3-D structures.

III. SEGMENTATION MODULE

Implementation of the segmentation module consists of 3 steps: (1) 2-D image segmentation of each CT slice to separate potential defect areas from clear wood, (2) morphological post-processing to remove spurious pixel clusters, and (3) 3-D connected volume growing to produce 3-D representations of potential defect areas. This module generates a 3-D image that highlights all the connected volumes that might represent defects. This image is passed to the scene analysis module for object recognition.

A. A 3-D Adaptive Smoothing Scheme

Growth rings are wood that is laid down annually around the stem of a tree in a radial fashion. They form a regular pattern of concentric rings of alternating density levels. Fig. 1 (upper left and lower right) show two CT images from two different red oak segments. On these images, the regular ring structure and defects, such as knots, decay and bark, can be clearly identified. As such, the growth rings obfuscate the segmentation and differentiation of important structures within a log. These annual rings not only adversely affect the quality of image segmentation, but they also adversely affect the object recognition task [41], making the analysis of log images a difficult task. Therefore, an important problem is how to filter out these rings while preserving other image details, e.g., small splits and holes. In this work, we developed an adaptive filter by extending the filter model proposed in [36]. In the following mathematical derivations, it is assumed that subscripts $i, j,$ and k are used to represent the $x, y,$ and z coordinates of a 3-D image. Then the observed image signal $x_{i,j,k}$ at (i, j, k) can be expressed by the sum of two uncorrelated components: the true signal $u_{i,j,k}$, and a corrupting noise $n_{i,j,k}$ with variance σ^2, i.e.,

$$x_{i,j,k} = u_{i,j,k} + n_{i,j,k}. \tag{1}$$

Filtering improves the signal-to-noise ratio at most points of an image. However, in regions of heavy edges or texture,
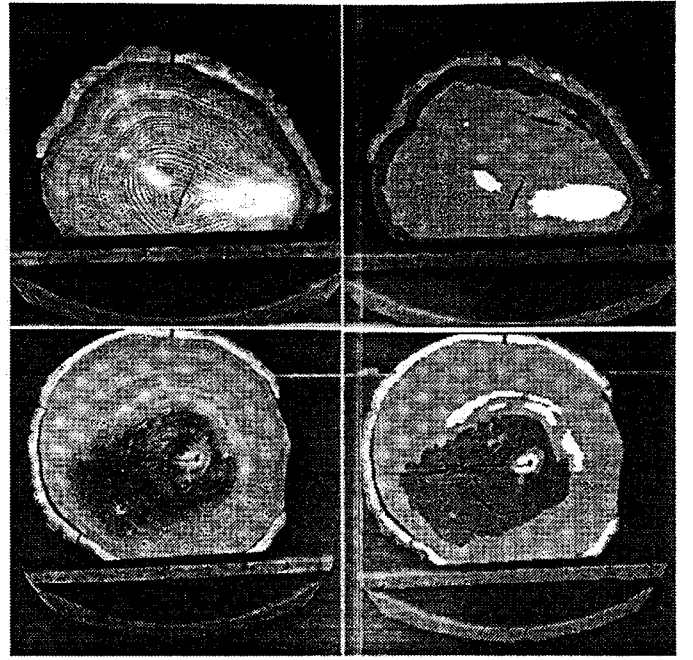

Fig. 1. (clockwise from upper left corner) Two sample CT images of red oak: Original red oak image and its segmented version. Another original red oak CT image and its segmented version.

filtering may degrade the signal more than it actually reduces the noise. In this case, a compromise would be not to do any filtering of the data. On the other hand, we may want to filter nontextured or nonedged areas. Accordingly, to obtain an optimal estimate, $z_{i,j,k}$, of the true image signal, $u_{i,j,k}$, a weighted sum of the observed signal, $x_{i,j,k}$, and a restored version, $y_{i,j,k}$, is constructed by

$$z_{i,j,k} = a_{i,j,k}x_{i,j,k} + b_{i,j,k}y_{i,j,k} \tag{2}$$

with $y_{i,j,k}$ defined as a convolution of $x_{i,j,k}$ and $h_{i,j,k}$, where $h_{i,j,k}$, called an initial filter, is a space-invariant operator. Note that $a_{i,j,k}$ and $b_{i,j,k}$ are the coefficients that are to be adjusted so that: (1) for edge regions, the noisy observation $x_{i,j,k}$ is retained by down weighting $y_{i,j,k}$, and (2) for nonedge regions, $y_{i,j,k}$ is retained by down weighting $x_{i,j,k}$.

It is noted that pixel $x_{i,j,k}$ on the kth slice is closely correlated with those on the $(k - 1)$th and $(k + 1)$th slices in a sequence of images. Hence, one way of improving filter performance is to find the solution for a least square problem defined in a finite 3-D volume. In solving this 3-D problem, filter coefficients $a_{i,j,k}$ and $b_{i,j,k}$ in (2) are computed from image data in consecutive slices of an image sequence. This extended 3-D filter also uses consecutive cross-sectional images to perform the initial image restoration on the pixels in a volume V. Operator $h_{i,j,k}$ can be chosen as the averaging filter as in [36], the 3-D Gaussian smoothing filter, or other nonlinear filters [41].

To compute the optimum filter coefficients $a_{i,j,k}$ and $b_{i,j,k}$, a least squares criterion is introduced to minimize the quadratic error over V

$$\epsilon^2(a, b) = \frac{1}{N_r} \sum_{(i,j,k) \in V} (z_{i,j,k} - u_{i,j,k})^2 \tag{3}$$

where V is defined as a cubic volume with dimension D_v, and N_r is the number of pixels in the volume V [41]. To find the optimum $a_{i,j,k}$ and $b_{i,j,k}$, let us assume, for the present, that these two coefficients are constant over the volume V, though later they are allowed to change at different spatial points. For simplicity, the subscripts i, j, and k for all the variables will be omitted in Equations 4–6. To retain the average intensity at a given point (i, j, k), the constraint $a + b = 1$ is added. This is equivalent to the constraint

$$g(a, b) = a + b - 1 = 0 \qquad (4)$$

that will be used in the minimization procedure.

Introducing a Lagrange multiplier λ to minimize error $\epsilon^2(a, b)$ under the constraint $g(a, b)$, we obtain the following criterion

$$e(a, b, \lambda) = \epsilon^2(a, b) + \lambda g(a, b). \qquad (5)$$

Taking partial derivatives of $e(a, b, \lambda)$ with respect to a, b and λ, and solving a set of simultaneous equations for $\{a, b, \lambda\}$, we have the following matrix equation

$$\begin{bmatrix} S_{xx} & S_{xy} & 1 \\ S_{yx} & S_{yy} & 1 \\ 1 & 1 & 0 \end{bmatrix} \begin{bmatrix} a \\ b \\ \lambda \end{bmatrix} = \begin{bmatrix} S_{ux} \\ S_{uy} \\ 1 \end{bmatrix} \qquad (6)$$

where terms with subscripts can be expressed by the following general expression

$$S_{xy} = S_{xy}(i, j, k) = \frac{\sum_{(i,j,k) \in V} x_{i,j,k} y_{i,j,k}}{V}. \qquad (7)$$

Solving (6) we obtain the optimal solutions for a and b defined by (5). The result is

$$a_{i,j,k} = 1 - \frac{(1 - \rho)\sigma^2}{P(i, j, k)}, \quad b_{i,j,k} = 1 - a_{i,j,k} \qquad (8)$$

where the constant ρ is equal to $h(0, 0, 0)$ when $h_{i,j,k}$ is an averaging filter. $P(i, j, k)$ is given by

$$P(i, j, k) = S_{(x-y)(x-y)}(i, j, k) > 0 \qquad (9)$$

which is a local estimate of the variance of the difference between the noisy and filtered signal that we refer to as the residue. This is a particularly simple implementation of the adaptive filter. Experiments [43] have indicated that the results obtained from this filter are better than those from other filters such as the σ-filter [20], and 2-D adaptive filter [36].

B. Image Segmentation Method

Given the strong variation in wood density among different types of defects and among different species of hardwood logs [43], one or more *fixed* thresholds are not appropriate for segmenting a log CT image into distinctive regions. In this study log images are thresholded on an slice-by-slice basis, using an *adaptive* multi-thresholding scheme similar to that in [11]. In this scheme, a histogram is first computed from each filtered image slice, then it is smoothed with a Gaussian function to eliminate spurious peaks. Thresholds are computed based on this smoothed histogram. According to
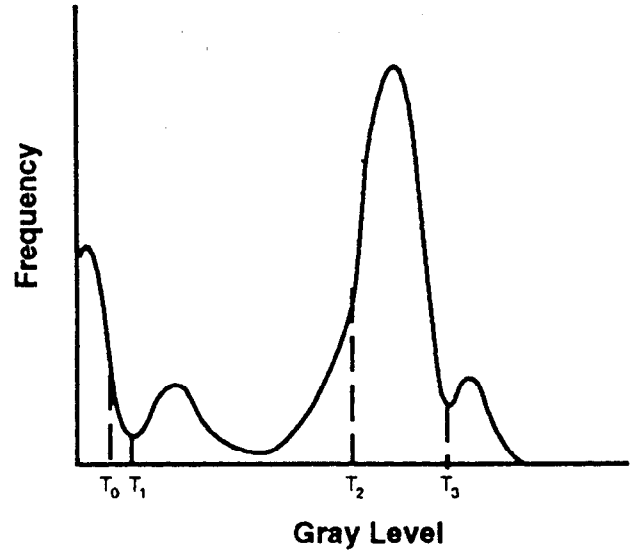

Fig. 2. A typical gray-level histogram of a CT log image with computed thresholds T_1, T_2, T_3 that can be used to separate CT image pixels into decay, clearwood, and knots.

[43] a log image contains pixels representing background, decay, splits, bark, knots, and clear wood. Because both bark and knots can have similar CT-numbers, they are temporarily treated like a single type of defect and will be separated by the object recognition module. Accordingly, three thresholds $\{T1, T2, T3\}$ are computed from the smoothed histogram $h(k)$ of an image. Fig. 2 shows a typical histogram of a CT log image that has been smoothed. Threshold T_0 is used to separate pixels that likely represent air surrounding the log or air that represents voids in the log. Note that since the density of air does not change, T_0 can be a fixed threshold. Thresholds T_1 and T_2 are used to separate pixels of likely decay and splits. Finally, thresholds T_2 and T_3 are used to separate pixels of likely bark and knots. These three threshold values are determined as follows:

1) T_1: $T_0 < T_1 < T_2 - D$, where T_0 and d are adjustable constants, e.g., $T_0 = 400, d = 50$.
2) $T_2 = k$, where k is defined by $h''(k) = \max h''(i)$ for all i, i.e., T_2 is the location where the second derivative of h(i) has a global maximum.
3) $T_3 = i$, where i is the location of the last zero-crossing of $h'(k)$, the first derivative of $h(k)$.

C. Morphological Post-Processing

Using the above thresholds, image segmentation produces a number of sizable, uniform 2-D areas that have jagged boundaries. These regions correspond to true wood defects. However, the segmentation also produces a small number of smaller spurious defect areas of different sizes. Morphological operations, such as erosion and dilation, are applied to a segmented image slice to eliminate rugged boundaries and spurious areas [42]. Let us denote a digital image by X, and a structuring element by B that is defined over on a finite mask Ω. In image erosion, a structuring element B scans through the image X in raster order, and it eliminates a pixel if none of its neighboring pixels in Ω has the same gray level as
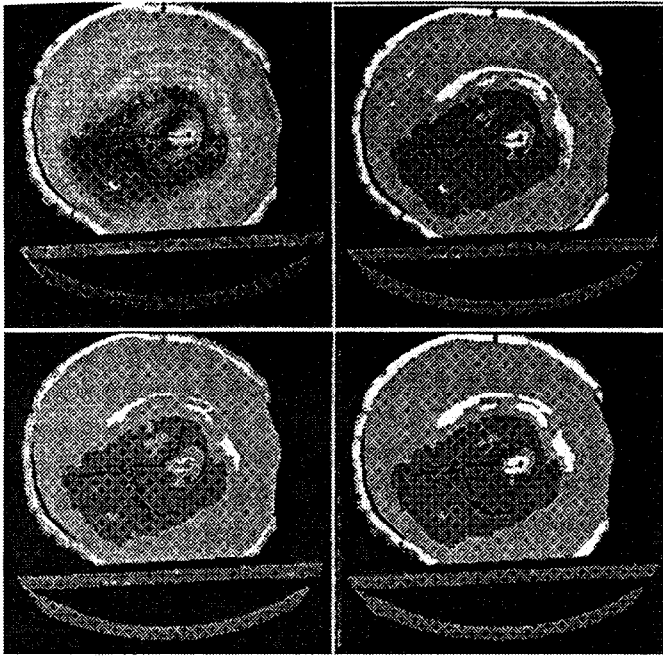
Fig. 3. (clockwise from upper left corner) Segmentation module operations: Original red oak CT image; its segmented version; after image erosion, and after image dilation.

it has. Whereas in image dilation, the gray levels of all the neighboring pixels in Ω are changed to that of the center pixel. These morphological masks B can be defined by a series of windows of size N by N, with $N = 3, 5, 7, \cdots$

In the prototype vision system, an image erosion operation is first performed on a segmented image slice to remove those small, spurious areas. Then an image dilation is performed to restore those pixels of the real defect areas that may have been eliminate by the erosion operation. These filtering segmentation and erosion-dilation procedures produce a number of uniform areas on each 2-D image. Fig. 3 demonstrates these two image morphological operations on a red oak image following segmentation. When consecutive image slices are grouped together, corresponding areas on different image slices are combined to form 3-D connected regions or volumes. This grouping into volumes provides 3-D shape information that is used by the defect recognition system to label each of the volumes found. In this study, the 2-D version of the connected component labeling (CCL) algorithm [30] was modified to create a 3-D version, called *3-D connected volume growing*, to group together individual 2-D areas on consecutive slices [41]. This grouping operation might create, however, some small, spurious volumes which do not correspond to any real defect object in a log. Therefore a volume thresholding process is adopted whereby each 3-D volume is compared against a preset value and all volumes with a number of pixels less than this value are automatically eliminated.

IV. SCENE ANALYSIS MODULE

After segmentation and 3-D volume growing, features, such as density, texture, geometric properties and geometrical relationships, of internal objects are computed from the 3-D imagery. These computed features are applied to defect recognition in the scene analysis module. In this module,

inexact knowledge is manipulated using the Dempster-Shafer model for reasoning under uncertainty, and the inference engine is based on the theory of evidential reasoning. Log CT images are rich in wood grain texture, which can aid the recognition task; however, texture analysis for defect detection is treated separately in [44].

In industrial automation, most current inspection methods are based on exact information about the object, and they tend to implement a simple form of the Bayesian discriminant in their decision process. In most practical cases, however, observations about objects are unreliable and incomplete, representation of objects is ambiguous, measurement can be imprecise, and propositions about hypotheses based on a collection of evidence are uncertain. Given the CT characteristics of wood defects [43], statistical or analytical classification procedures alone are difficult to successfully implement. Less exacting methods are required in this scene analysis problem [3], [28]. To mitigate these difficulties, we have applied a heuristic, knowledge-based recognition system, as described in [5] for identifying surface defects in sawn lumber. That system has been successful in recognizing several types of defects on a large number of boards from a variety of different hardwood species. It effectively combines domain-independent, low-level image features with domain-specific heuristics to create a general recognition scheme.

The scene analysis module is comprised of the following three steps: (1) compute image features from connected volumes produced by the segmentation module, (2) apply a set of hypothesis tests to each object using the D-S model, and (3) perform object recognition by evidential reasoning.

A. The Basic Feature Set for Wood Defect Identification

After the 3-D connected volume growing operation, the scene analysis module extracts a vector of basic features from each of the 3-D connected volumes. The set of basic features captures intensity- (i.e., density-) and orientation-related properties of the various internal log defects, and, hence, are features that can be used to label the 3-D volumes. Let us denote an original 3-D CT image by $G(x, y, z)$. The pixels of $G(x, y, z)$ have intensities ranging from 0 to 2047. Let $O(x, y, z)$ denote a 3-D connected volume found by the connected volume growing operation. $O(x, y, z)$ has the same spatial dimensions as $G(x, y, z)$ but if $O(x, y, z)$ is the kth connected volume found then $O(x, y, z) = k$ when (x, y, z) is in this connected volume and $O(x, y, z) = 0$ otherwise. Also let the number of pixels in this connected volume, i.e., the number of pixels where $O(x, y, z) = k$, be denoted by the integer V. After a gray level conversion, each connected volume $O(x, y, z)$ can be decomposed into N binary functions $b_i(x, y), i = 1, 2, \cdots, N$, where N is the number of slices spanned by the object in the z direction. The values of these binary functions $b_i(x, y)$ are 1 for $(x, y) \in R_i$, and 0 elsewhere, where R_i is the 2-D cross section of the connected volume in slice i. From each connected volume $O(x, y, z)$, a set of 7 basic features $f_i(i = 1, 2, \cdots 7)$ are extracted. These *basic features* are:

Average_Angle (Φ): The average angle is defined as the average of $N - 1$ angles $\theta_i(i = 1, 2, \cdots, N - 1)$, where θ_i is

spanned by the x-y plane and a line connecting the centroids of two adjacent slices, expressed as

$$\Phi = \frac{1}{N-1} \sum_{i=1}^{N-1} \theta_i \quad \text{where } \theta_i = \arctan\left(\frac{dz}{D_i}\right) \quad (10)$$

where dz is the slice spacing (which is 8 mm for the CT scanner used in this work), and D_i is the shift in centroid on the x-y plane from slice i to slice $i+1$. For the two centroids at (x_i, y_i) and (x_{i+1}, y_{i+1}) on the two slices, D_i is computed as the distance $D_i = \sqrt{(x_{i+1} - x_i)^2 + (y_{i+1} - y_i)^2}$.

Compactness (C): The compactness of a 3-D connected volume is defined as the ratio of its surface area (S) to its volume (V), i.e.,

$$C = \frac{S}{V} \quad (11)$$

where S is the number of boundary pixels and where V is defined as above.

Average_Elongation (E): The average elongation of a 3-D connected volume is the average of the 2-D elongations, $E_i, i = 1, \cdots, N$, of the corresponding N planer regions in the object, expressed by

$$E = \frac{1}{N} \sum_{i=1}^{N} E_i$$

where

$$E_i = \frac{\sqrt{M_{2,0}(i) - M_{0,2}(i)} + 4M_{1,1}(i)}{M_{0,0}(i)} \quad (12)$$

and

$$M_{m,n}(i) = \sum_{(x,y)} (x - x_0)^m (y - y_0)^n b_i(x, y)$$

$$\text{for } m, n = 0, 1, 2$$

where $M_{mn}(i)$ is the mnth order central moment about the centroid (x_0, y_0) of the ith binary function $b_i(x, y)$.

Area_Variation (A): This shape-related feature is the normalized variance of the area values of the N slices belonging to the 3-D connected volume, and it is defined as

$$A = \frac{Var\_S_{\text{area}}}{Avg\_S_{\text{area}}} \quad (13)$$

where Var_S_{area} and Avg_S_{area} are respectively the variance and average of the area values that are computed from these N slices.

Object_Intensity_Ave (μ): This feature is defined as the average pixel intensity of a connected volume

$$\mu = \frac{1}{V} \sum_{(x,y,z) \in O} G(x, y, z). \quad (14)$$

Object_Intensity_Var (s): This intensity-related feature is defined as the standard deviation of the pixel intensity (CT number) of a connected volume, and it is calculated by

$$s = \sqrt{\frac{\sum_{(x,y,z) \in O} (G(x,y,z) = \mu)^2}{V}}. \quad (15)$$

Moment_of_Inertia (I): This shape-related feature is calculated as follows:

$$I = \sum_{(x,y,z) \in O} [(x - x_0)^2 + (y - y_0)^2] G(x, y, z). \quad (16)$$

where x_0 and y_0 are the x and y coordinates of the centroid of the 3-D object.

B. Imperfect Knowledge Representation: The D-S Model

Defect recognition is conducted by passing each connected volume through a number of hypothesis tests that are implemented as production rules (IF-THEN statements). The *basic features* $f_i, i = 1, 2, \cdots, 7$, defined in the previous section, are used in the test set Π of the scene analysis module. There are 7 tests in Π, and they are denoted by

Π_Φ, *Average_Angle*
Π_C *Compactness*
Π_E, *Average_Elongation*
Π_A, *Area_Variation*
Π_μ, *Object_Intensity_Ave*
Π_s, *Object_Intensity_Var*
Π_I, *Moment_of_Inertia*.

These tests Π are applied in different combinations to the various 3-D connected volumes. The output from each of these tests provides the vision system partial evidence to support or refute a hypothesis about the identity of a volume. Based on partial evidence, the vision system arrives at a *consensus*-a final decision on the identity of the defect, by using Dempster's rule of *evidence combination* [9].

In the D-S theory of evidence, a frame of discernment Θ is defined as a finite set of mutually exclusive hypotheses. For a specific task, a set is a frame of discernment, if (1) its elements are interpreted as all possible answers to a question, and (2) exactly one of these elements is the correct answer. For the wood defect inspection problem under study, all possible answers to the question "what is the identity of this 3-D connected volume?" can be enumerated. The possible answers are: knot, split, pith, bark, stain, decay, and hole. It is noted that clear wood is not included in the frame of discernment because it can be readily classified by its volume, which is much larger than the volumes of any defects. Therefore, the frame of discernment in this case is

$$\Theta = \{\text{knot, split, pith, stain, decay, hole}\}. \quad (17)$$

Any subset X of Θ, $X \subset \Theta$, is a hypothesis about the answer to the question, i.e., about the identity of a connected volume (defect). For instance, when applied to a connected volume some of the tests Π_i generate evidence that the identity of the object could be $\{\text{knot}\}$, $\{\text{decay}\}$, or $\{\text{decay}\} \cup \{\text{knot}\}$.

Note that the 3-D connected volume's identity could be either knot or decay based on partial information extracted from the volume. In Bayesian reasoning, the posterior probability changes as evidence is acquired [10]. Likewise, in D-S theory, the belief in evidence may vary. It is customary in D-S theory to think about the degree of belief in evidence as analogous to the mass of a physical object, i.e., the mass of evidence that supports a belief. The evidence measure, symbolized by the

letter m, is analogous to the amount of mass. Associated with each piece of evidence is a basic probability assignment (*bpa*), denoted as function $m(X)$, that represents the impact of the evidence on the subsets of Θ, i.e., the probability assigned to the subset X. The quantity $m(X)$ can be viewed as the portion of total belief assigned exactly to X. The function $m(X)$ maps the power set of $\Theta(2^\Theta)$ to values between 0 and 1. This mapping is formally expressed as

$$m\colon P(\Theta) \to [0, 1]. \tag{18}$$

According to the D-S theory, the *bpa* must satisfy the following two properties:

1) the basic probability assignment of a null event $\varnothing$ is 0, $m(\varnothing) = 0$; and
2) the sum of the *bpa*'s for all subsets of Θ must be 1.

D-S theory does not force belief to be assigned to ignorance or refutation of a hypothesis. Instead, the belief or mass determined by the *bpa* mapping function $m(X)$ is assigned only to those subsets of the frame of discernment Θ, called *focal elements* of Θ, to which one wishes to assign nonzero belief. Any belief that is not assigned to a specific subset is considered *no belief* or *nonbelief* and is just associated with Θ. Belief that refutes a hypothesis is *disbelief*, which is distinct from nonbelief.

In our scene analysis module, each of the seven tests in the test set $\Pi = \Pi_\Phi, \Pi_C, \Pi_E, \Pi_A, \Pi_\mu, \Pi_s, \Pi_I$ maps the evidence that is extracted from the detected objects into a *bpa* $m_i(\cdot)$, a set of discrete mass values between 0 and 1, i.e.,

$$m_i(X) = [0, 1] \text{ for any } X \subset \Theta, \qquad i = 1, 2, \cdots, 7. \tag{19}$$

where $m_i(\cdot)$ could be replaced by one of the *bpa* mapping functions $\{m_\Phi(\cdot),\ m_C(\cdot),\ m_E(\cdot),\ m_A(\cdot),\ m_\mu(\cdot),\ m_\sigma(\cdot), m_I(\cdot)\}$, depending on the particular test used. In general, each test Π_i is a function of a measurement made on the object (by the basic feature f_i) and a parameter vector $\vec{T}_i$, i.e.

$$\Pi_i = g_i(f_i, \vec{T}_i). \tag{20}$$

The parameter vectors $\vec{T}_i$ consist of a set of thresholding values that represent delimiting points for different ranges of the g_i functions. These values are determined either from training examples in an image data base, or by experts in the field of hardwood log grading.

In the knowledge base, the *bpa*'s are implemented as a set of discrete table look-up functions embedded in the vision system. Evidential strengths are extracted by consulting these look-up tables. For instance, the two tests that are designed to hypothesize knots are the Average_Angle test Π_Φ and the Area_Variation test Π_A. Associated with these two tests are two evidence mapping functions, $m_\Phi(\cdot)$ and $m_A(\cdot)$, together with the corresponding parameters t_Φ and t_A. These two *bpa* mapping functions are defined respectively by

bpa Mapping Function $m_\Phi(\cdot)$ by Test Π_Φ:

if $(T_\Phi > t_\Phi)$

$$m_\Phi(X) = \begin{cases} 0.9 & X = \{\text{knot}\} \\ 0.05 & X = \{\text{decay}\} \\ 0.05 & X = \{\Theta\} \end{cases}$$

else

$$m_\Phi(X) = \begin{cases} 0.1 & X = \{\text{knot}\} \\ 0.6 & X = \{\text{bark}\} \cup \{\text{decay}\} \\ 0.3 & X = \{\Theta\} \end{cases}$$

bpa Mapping Function $m_A(\cdot)$ by Test Π_A:

if $(T_A > t_A)$

$$m_A(X) = \begin{cases} 0.9 & X = \{\text{knot}\} \\ 0.1 & X = \{\Theta\} \end{cases}$$

else

$$m_A(X) = \begin{cases} 0.6 & X = \{\text{bark}\} \cup \{\text{decay}\} \\ 0.4 & X = \{\Theta\}. \end{cases}$$

The *bpa*'s for other tests all have the format similar to the above examples [43].

C. Object Recognition by Evidential Reasoning

As stated above, there are seven tests that target different types of hardwood log defects. For example, the *Average_Angle* test Π_Φ is designed to inspect knots, and the *Compactness* test Π_C detects pith, and so forth. To recognize a candidate object with minimal computation, our vision system employs a *focus of attention* mechanism. For each object produced by the segmentation module, the Object_Intensity_Ave test Π_μ is applied first. The purpose of this test is to coarsely divide the clear wood and defects into 3 groups of candidate objects according to their CT-numbers: Group 1—knots and bark with the highest CT numbers, Group 2—clear wood, decay and sta n with medium CT numbers, and Group 3—splits, holes and pith with the lowest CT numbers. This division into groups does not alleviate the problem of distinguishing between group members. For example, knots may have the same average CT-number as bark, and stain may have the same CT-number as clear wood. Nevertheless, this test does provide a valuable, initial classification.

Next, a subset of Π is applied to objects belonging to one of the 3 groups of candidate objects. Responses to each of these tests provide partial evidence (also called evidence strength) to different hypotheses about the identity of objects. Note that results of tests from Π may logically conflict, but others may verify a hypothesis. D-S theory selects a belief function that is able to synthesize all partial knowledge and to achieve a multi-criteria optimization. Evidence provided by each test Π_i is represented as a *bpa* over a hypothesis space spanned by Θ. An individual hypothesis, such as $X = \{$the connected volume is a knot$\}$ is supported or refuted depending on the response of a connected volume to its corresponding tests. Each such test Π_i merely contributes to the overall support, and the effect of Π_i on a hypothesis is determined by its *evidential strength* or degree of confirmation. An inference network that propagates evidence strength can then be constructed using Dempster's rule of combination [9].

Let m_1 and m_2 be the *bpa* of two independent pieces of evidence obtained by applying two tests Π_1, and Π_2 to one object. Also let X and Y denote any two subsets of the frame of discernment $\Theta, X \subset \Theta$, and $Y \subset \Theta$. We denote $m(Z)$ as a new belief function that is obtained by synthesizing the two pieces of partial evidence $m_1(X)$ and $m_2(Y)$ from these two

independent tests. Because Dempster's rule of combination is commutative and associative, $m_1(X)$ and $m_2(Y)$ can be combined regardless of order. calculated Using Dempster's rule of combination, the new $bpa\, m(Z)$, for any $Z \subset \Theta$, can be given by

$$m(Z) = \begin{cases} K \sum_{X \cap Y = Z} m_1(X)m_2(Y) & \text{if } Z \neq \varnothing \\ 0 & \text{if } Z = \varnothing \end{cases} \quad (21)$$

where K is a normalization factor [18]

$$K = \frac{1}{1 - \sum_{X \cap Y = \varnothing} m_1(X)m_2(Y)} \quad (22)$$

When there are more than two tests, the above rule of evidence combination still can be used. Each time a pair of m_i's is combined, the resulting bpa is combined with the bpa generated by the next test. The same procedure can be applied $N - 1$ times until all $N bpa$'s have been combined.

At the final stage of reasoning, a single hypothesis establishes defect identity, if and only if its belief function has a maximum value that is greater than T_Θ, a threshold specified in the knowledge base. The connected volume is recognized as defect type i if the discrete value of the combined $bpa\, m(X_i)$ is maximum and it is above the threshold T_Θ.

Due to the limited number of log images available, the actual frame of discernment Θ in this study is smaller than that given in (17). It consists of a finite number of exhaustive and mutually exclusive subsets, each of which is one of the following hypotheses: (1) {An object is a knot}, denoted as $\{K\}$, (2) {An object is decay, i.e. "rot"}, denoted as $\{R\}$, and (3) {An object is bark}, denoted as $\{B\}$.

In experiments, the threshold vectors T_i associated with each test Π_i are, at present, determined by observation. In addition, the threshold value T_Θ, which is used to select a single hypothesis from final evidence strengths, is specified in the knowledge base, and it is set to $T_\Theta = 0.5$. This means, when belief for a hypothesis is maximum among all hypotheses and is greater than or equal to 0.5, that hypothesis is selected. Once the identity of each defect in a log has been determined by this scene analysis module, this identity information, along with each defect's location, size, density and minimum bounding volume, can be output to a data file. This defect information could then be used as input to software that calculates the best cutting pattern for the log. In a further stage of sawmill automation, this cutting pattern, also in the form of a data file, could be passed to a controller unit, that would automate the necessary positioning operations at the headrig to faithfully execute the chosen sawing pattern.

V. RESULTS

One segment from a red oak log and one segment from a yellow poplar log were selected as the test set. This test set consists of 2 sequences of yellow poplar images and 3 sequences of red oak images, with each sequence having 10 to 20 CT slices. They contains the following defects: four bark regions, six knot regions and two decay regions. Since there are three types of defects available in the test set, only
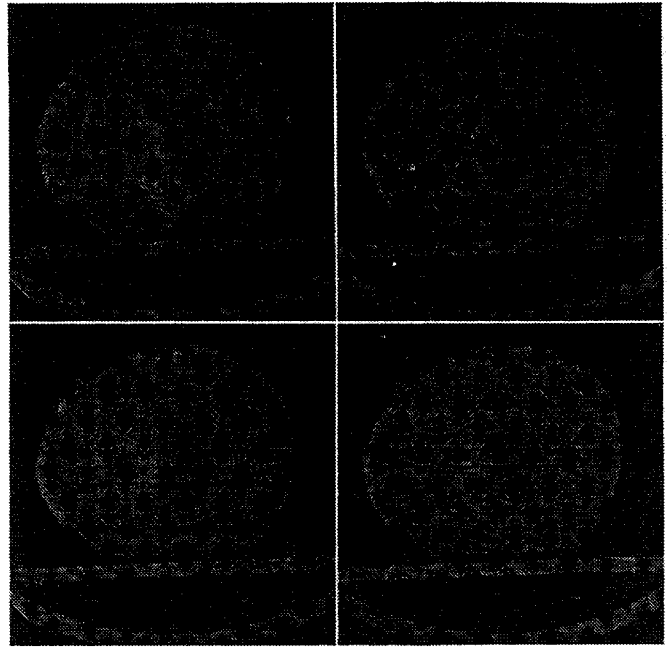

Fig. 4. (clockwise from upper left corner) Four consecutive CT slices of a red oak log.

four tests Π_μ, Π_Φ, Π_I, and Π_A were used. However, when additional image data becomes available, the remaining three tests (or other new tests) can be added easily, making the scene analysis module more reliable. Experimental results from one of the image sequences in the test set are described below.

Figs. 4–7 illustrate the object recognition procedure on four consecutive slices of a red oak log. The original CT imagery appears in Fig. 4. Fig. 5 contains the segmentation results for the corresponding images and Fig. 6 presents the results of 3-D volume growing within 2-D images. Potential defect objects are distinguished from clear wood and are represented by different shading. Although the object near the log center has been segmented into several pieces, connected component labeling organizes the pieces into one object.

We will use this example to demonstrate how bpa's are combined to arrive at the labeling for the objects in Fig. 7. Let us consider the three bpa's $m_I(\cdot), m_A(\cdot)$ and $m_\Phi(\cdot)$ after applying three tests Π_i, Π_A and Π_Φ to the object near the center of the log segment in Fig. 4. First, this object was categorized as a *group 1* object (knot or bark) by the focus of attention mechanism, i.e., the *Object_Intensity_Ave* test Π_μ. Then three additional tests Π_I, Π_A and Π_Φ were applied. The three $bpa' s m_I(\cdot), m_A(\cdot)$ and $m_\Phi(\cdot)$ associated with these three tests are implemented as discrete table look-up functions that are listed in Table I, where letters K, B, and R represent knot, bark, and decay (rot) respectively. Thresholding values associated with these three tests are t_I, t_A and t_Φ. Using log images available from the data base, these thresholds were determined to be $t_I = 100, t_A = 50$, and $t_\Phi = 15$, respectively. For object recognition, the inference engine first propagated the evidence by combining together the two bpa's, $m_I(\cdot)$ and $m_A(\cdot)$, into a new bpa denoted by $m_{IA}(\cdot)$, which is listed in Table I.

Then, $m_{IA}(\cdot)$ was combined with $m_\Phi(\cdot)$, resulting in a new bpa function, $m_{IA\Phi}(\cdot)$, as shown in Table I. The final
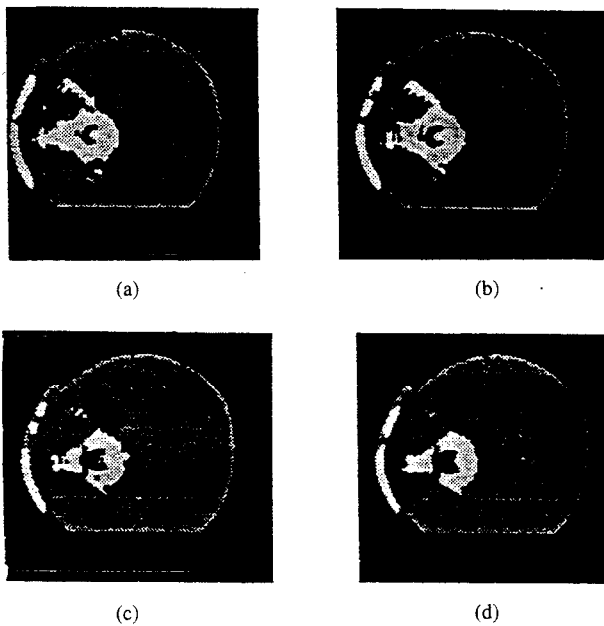
(a)   (b)

(c)   (d)

Fig. 5. The segmentation results of the of the red oak images in Fig. 4, showing the segmented version of the corresponding images in in Fig. 4.

slice 1   slice 2

slice 3   slice 4

Fig. 7. Object recognition results obtained from the data shown in Fig. 6.
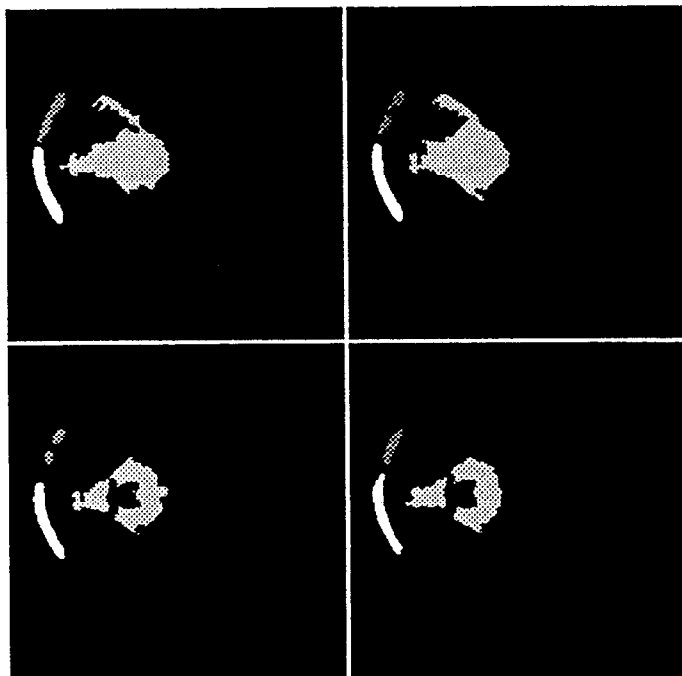

Fig. 6. Results of 3-D volume growing applied to the images in Fig. 5,. Note that each object assigned a distinct identification number, distinguished by different shading.

TABLE I
VALUES OF THE VARIOUS bpa FUNCTIONS THAT WERE
CALCULATED USING THE EXAMPLE IN THE TEXT

	{B}	{K}	{R}	{RB}	{KB}	{Θ}
$m_A(.)$					0.80	0.20
$m_I(.)$				0.60		0.40
$m_\Theta(.)$		0.90	0.05			0.05
$m_{IA}(.)$	0.48			0.12	0.32	0.08
$m_{IA\Theta}(.)$	0.057	0.838	0.024	0.014	0.038	0.009

bpa for the hypothesis knot (K) has the maximum evidence strength (0.838) which is greater than the preset threshold value $T_\Theta = 0.5$. This hypothesis is accepted and the vision system correctly identifies the object near the log center as a knot (K). Note that, if only partial evidence (from two tests Π_I and Π_A) were used in the decision-making process, the system would have incorrectly hypothesized the object to be bark (B), since the hypothesis of bark has the maximum evidence strength (0.48) in $m_{IA}(\cdot)$ given in Table I. Because
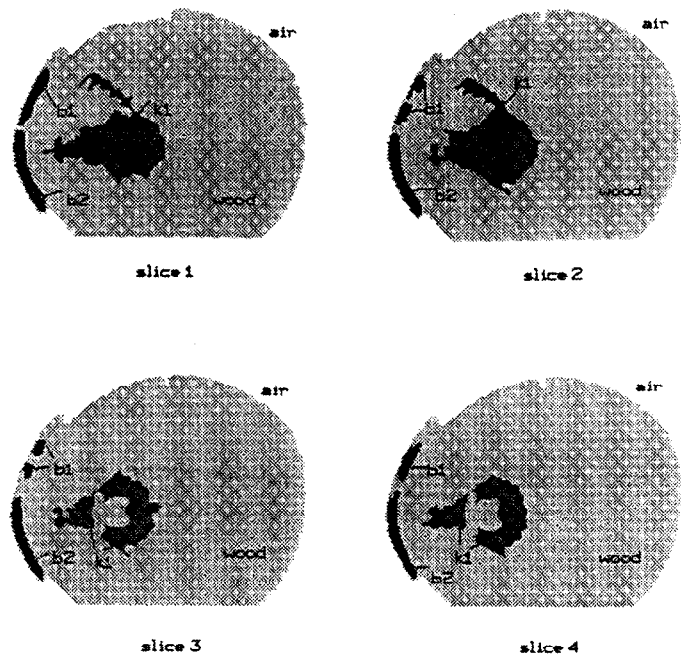
the strength value of $m_{IA}(\cdot)$ would not surpass the threshold, however, it would not lead to an incorrect identification in this case. The same procedure of evidence pooling was applied to the thin object on the boundary of the log segment (Fig. 6), and this defect was correctly classified as bark (B). Complete recognition results for this series of images appear in Fig. 7.

VI. CONCLUSIONS

This paper describes the software components of a prototype vision system for hardwood log inspection that uses CT imagery. To efficiently separate defects from clear wood, an adaptive filter eliminates annual rings in CT images while preserving important details. Images are segmented on a slice-by-slice basis using a dynamic multi-thresholding scheme. Connected volume growing generates 3-D connected volumes from the 2-D segmented cross-sections. A knowledge-based approach classifies 3-D objects using both domain-independe t features and domain dependent heuristics. It uses a set of basic features that are incorporated into hypothesis tests. To cope with imprecision and uncertainty in representi g defect information, the Dempster Shafer model was adopted for inexact reasoning.

Using a limited data set for two species of logs, the proposed vision system seems able to recognize log defects with irregular 3-D shapes. Experimental results indicate that the image segmentation module can separate clear wood from knots, splits, holes, decay, and bark. The scene analysis module can recognize knots, decay, and bark. These methods seem to be robust and species independent. Consequently, this work demonstrates that a CT-based machine vision system can be developed to locate and identify internal defects of hardwood logs. It is possible that this general methodology could also be used with other imaging modalities, such as MRI and ultrasound, and in other industrial inspection applications by modifying various features, thresholds, and tests.

It can be seen (Fig. 1) that the filtering operation eliminates log pith in the imagery. Because the prototype vision system does not use pith to extract any information about internal defects, its elimination does not impact recognition performance. In [32] a different approach was used for Australian hardwoods, where pith location was detected on the image and used to calculate the percentage of heartwood in sawn timber. Our system does not use pith for recognition because pith is not always at the center of North American hardwoods. In the absence of pith, however, computational methods such as moment-based algorithms could be used to find the center of inertia of a log regardless of the performance of the image segmentation module.

Nevertheless, this prototype system has a number of significant limitations and, clearly, further research is needed to fully address the log inspection problem. First, as is apparent from Fig. 6 and Fig. 7, more work needs to be done to improve circumscription of defect boundaries. In some cases segmentation has been too liberal and in other cases it has been too conservative. Second, in addition to accuracy increases for those defect types for which some competence already exists, we must expand the system's capabilities to other defect types. Third, the system also needs testing on other species, on logs of varying moisture content, and with higher-quality logs containing smaller defects. Fourth, the existing algorithms are computationally demanding, benchmark tests can be used to determine how viable they are for eventual, real-time implementation. Finally, wood texture models were developed by [44] and could be incorporated into a wood texture test for use in the scene analysis module. The expectation is that a texture test would provide valuable additional knowledge for better discernment of defect types.

This vision system, based on CT imagery, is a first attempt at automating internal characterization of logs. As nondestructive evaluation (NDE) methods become economically practical for the forest products manufacturing industry, the problem of what to do with NDE data will become very important. Systems like the one presented here will become obligatory if NDE data are to be useful and their expense justified.

REFERENCES

[1] D. M. Benson-Cooper, R. L. Knowles, F. J. Thomas, and D. J. Cown, "Computed tomographic scanning for detection of defects within logs," Forest Research Institute, New Zealand Forest Service, Bulletin no. 8, 1992.

[2] R. Birkeland and W. Han, "Ultrasonic scanning for internal log defects," Proc. 4th Int. Conf. on Scanning Technology in The Wood Industry, Oct., 1991.

[3] B. Buchanan and E. Shortliffe, Rule-Based Expert Systems: The MYCIN Experiments of the Stanford Heuristic Programming Project. Reading, MA: Addison-Wesley, 1984.

[4] S. J. Chang, M. Cohen and P. C. Wang, "Ultrafast scanning of hardwood logs with an NMR scanner," Proc. 4th Int Conf. on Scanning Technology in The Wood Industry, Oct., 1991.

[5] T-H. Cho, R. W. Conners and P. Araman, "A computer vision system for automatic lumber detection using blackboard expert system method," Proc. 10th Int. Conf. on Pattern Recognition, Atlantic City, NJ, June, 1990.

[6] T-H. Cho "A knowledge-based machine vision system for automated industrial web inspection," Doctoral Degree Dissertation, Dept. of Electrical Engineering, Virginia Polytechnic Institute & State University, Blacksburg, May 1991.

[7] R. W. Conners, et al., "Identifying and locating surface defects in wood: Part of an automated lumber processing system," IEEE Trans. Pattern Anal. Machine Intell., vol. PAMI-5, no. 6, pp. 573–583, Nov. 1983.

[8] J. Davis and P. Wells, "Computer tomography measurements on wood," Indus. Metrology, 1991.

[9] A. P. Dempster, Ann. Math. Stat., vol. 38, pp. 325–423, 1967.

[10] R. Duda, P. Hart, and R. Reboh, "A computer-based consultant for mineral exploration," Tech. Rep., SRI International, Menlo Park, CA, 1979.

[11] B. V. Funt and E. C. Bryant, "A computer vision system that analyzes CT-scans of sawlogs," Proc. of IEEE Conf. on Computer Vision and Pattern Recognition, pp. 175–177, 1985.

[12] B. V. Funt and E. C. Bryant, "Detection of internal log defects by automatic interpretation of tomographic images," Forest Prod. J., Vol. 37, no. 1, pp. 56–62, 1987.

[13] S. Grundberg and A. Gronlund, "Log scanning—extraction of knot geometry," Proc. of the Seminar/Workshop on Scanning Technology and Image Processing on Wood, Skellefta, Sweden, Aug. 30–Sept. 31, 1992.

[14] T. Harless, F. Wagner, F. Taylor, V. Yadama, and C. McMillin, "Methodology for locating defects within hardwood logs and determining their impact on lumber-value yield," Forest Prod. J., vol. 41, no. 4, pp. 25–30, 1991.

[15] Y. Hattori and Y. Hanaga, "Non-destructive measurements of moisture distribution in wood with a medical X-ray CT scanner I: accuracy and influence factors," Mokuzai Gakkaisha, vol. 13, pp. 974–980, 1985.

[16] S. J. Henkind and M. Harrison, "An analysis of four uncertainty calculi," IEEE Trans. Syst., Man, Cybern., vol. 18, no. 5, pp. 700–714, 1988.

[17] D. G. Hodge, W. C. Anderson, and C. W. McMillin, "The economic potential of CT scanner for hardwood sawmills," Forest Prod. J., vol. 40, no. 3, pp. 65–69, 1990.

[18] J. Gordon and E. Shortliffe, "The MYCIN experiments of the Stanford heuristic programming project," in Rule-Based Expert Systems, Ed. B. Buchanan and E. Shortliffe. Reading, MA: Addison-Wesley, 1985.

[19] S. Grundberg and A. Gronlund, "Methods for reducing data when scanning for internal log defects of hardwood logs with an NMR scanner," Proc. 4th Int. Conf. on Scanning Technology in The Wood Industry, San Francisco, CA, Oct., 1991.

[20] A. K. Jain, Fundamentals of Digital Image Processing. Englewood Cliffs, NJ: Prentice-Hall, 1989.

[21] E. A. King, "An operating defect detector," presented at The North American Sawmill and Plywood Clinic, Portland, OR, Mar., 1979.

[22] D. E. Kline, personal communication, Department of Wood Science and Forest Products, Virginia Polytechnic Institute and State University, 1990.

[23] A. Koivo and C. Kim, "Robust image modeling for classification of surface boards," IEEE Trans. Syst., Man, Cybern., vol. 19, no. 6, pp. 1659–1666, Nov/Dec., 1989.

[24] S. C. Lee, G. Qian, J. Chen and Y. Sun, "Determine a maximum value yield of a log using an optical log scanner," Proc. IEEE Conf. on Computer Vision and Pattern Recognition, Meno, HI, Jan., 1991.

[25] F. B. Malcolm, "Effect of defect placement and taper setout on lumber grade yields when sawing hardwood logs," Tech. Rep. 2221, USDA Forest Service Forest Products Laboratory, Madison, WI, p. 7, 1956.

[26] P. Martin, R. Collet, P. Barthelemy, and G. Roussy, "Evaluation of wood characteristics: internal scanning of materials by microwave," Wood Sci. Technol., vol. 21, no. 4, pp. 361–371, Apr., 1987.

[27] L. G. Occena and J. M. A. Tanchoco, "Pattern directed extraction and characterization of defect configurations in solid log models," Artif. Intell. Eng., vol. 4, no. 3, pp. 144–154, Mar., 1989.

[28] J. Pearl, "On Evidential Reasoning in a hierarchy of hypotheses," Artif. Intell., vol. 28, pp. 9–15, 1986.

[29] G. D. Shaffer, *A Mathematical Theory of Evidence*. Princeton, NJ: Princeton Univ. Press, 1976.

[30] Y. Shirai, *3-Dimensional Computer Vision*. New York: Springer-Verlag, 1987.

[31] S. Som, P. Wells and J. Davis, "Automated feature extraction of wood from tomographic images," *Proc. ICARV'92, Second Int. Conf. on Automation, Robotics and Computer Vision*, Singapore, Vol. 1, pp. CV-14.4.1 to XCV-14.4.5, Sept. 16–18, 1992.

[32] S. Som, J. Davis, P. Wells and I. Svalbe, "Morphological methods for processing tomographic images of wood," *Proc. DICTA-93, Conf. on Digital Image Computing: Techniques and Applications*, Sydney, Australia, Dec. 8–10, Vol. II, pp. 564–571, 1993.

[33] P. H. Steele and F. W. Taylor, "Hardwood sawing methods to maximize value and volume: preliminary results," *Proc. 7th Annu. Hardwood Symp.*, U.S. Hardwood Research Council, pp. 149–157, May, 1989.

[34] T. M. Strat and M. A. Fischler, "Context-based vision: recognizing objects using information from both 2-D and 3 d imagery," *IEEE Trans. Pattern Analy. Machine Intell.*, vol. 13, no. 10, pp. 1050–1065, Oct., 1991.

[35] F. Taylor, F. Wagner, C. McMillin, I. Morgan, and F. Hopkins, "Locating knots by industrial tomography—a feasibility study," *Forest Prod. J.*, vol. 34, no, 5, pp. 42–46, 1984.

[36] M. Unser, "Improved restoration of noisy images by adaptive least-squares post-filtering," *Signal Processing*, vol. 20, no. 1, pp. 3–14, May 1990.

[37] F. Wagner, F. Taylor, D. Ladd, C. McMillin and F. Roder, "Ultrafast CT scanning of an oak log for internal defects," *Forest Prod. J.*, vol. 39, Nov./Dec., 1989.

[38] F. Wagner, T. Harless, P. Steele, F, Taylor, V. Yadame, and C. W. McMillin, "Potential benefit of internal-log scanning," *Proc. Process Control/Production Management of Wood Product Technology for the 90's*, Athens, GA, Oct. 30–Nov. 1, pp. 77–88, 1990.

[39] P. C. Wang, S. J. Chang and J. Olson, "Scanning logs with an NMR scanner," *Proc. 7th Int. Nondestructive Testing of Wood Symposium*, pp. 209–219, Sept. 1989.

[40] P. Wells, S. Som, and J, Davis, "Automated feature extraction from tomographic images of wood," *Proc. of DICTA 91, Digital Image Computing: Techniques and Applications*, Melbourne, Victoria, Australia, pp. 198–193, Dec. 1991.

[41] D. Zhu, R. W. Conners, and P. Araman, "3-d signal processing in a computer vision system," *Proc. IEEE Int. Conf. on Systems Engineering*, Dayton, OH, Aug. 1–3, 1991.

[42] D. Zhu, R. Conners, F. Lamb, P. Araman, and D. Schmoldt, "A computer vision system for locating and identifying internal log defects using CT imagery," *Proc. 4th Int. Conf. on Scanning Technology in Sawmilling*, San Francisco, CA, pp. 1–13, Oct., 1991.

[43] D. Zhu, "A feasibility study on using CT image analysis for locating and identifying hardwood defects," Ph.D. Dissertation, Department of Electrical Engineering, Virginia Polytechnic Institute and State University, Blacksburg, Apr. 1993.

[44] D. Zhu and A. A. Beex, "Robust spatial autoregressive modeling for hardwood log inspection," *J. Visual Comm. Image Representation*, vol. 5, no. 1, pp. 41–51, Mar., 1994.

Richard W. Conners (M'73) received the B.A. and M.A. degrees in mathematics in 1968 and 1972, respectively and the Ph.D. degree in electrical engineering, all from the University of Missouri, Columbia.

His work experience includes one and a half years with the Bioengineering and Advanced Automation Program, University of Missouri, eight years with the Remote Sensing and Image Processing Laboratory, Louisiana State University, Baton Rouge, Louisiana, and seven years with the Spatial Data Analysis Laboratory, Virginia Polytechnic Institute and State University, Blacksburg. At each of these institutions he also held positions within the electrical engineering departments. His research interest is in developing machine vision systems for automatic inspection, including both the software and hardware components of such systems. Areas of expertise include computer vision, digital design, artificial intelligence, and pattern recognition.

Daniel L. Schmoldt received the B.S. degree in mathematics in 1976, the M.S. degree in forestry in 1980, the M.S. degree in computer science in 1983, and the Ph.D. degree in forest biometry in 1987, all from the University of Wisconsin, Madison.

Since 1987, he has been with the USDA Forest Service. From 1987 to 1991, he was with Pacific Southwest Research as a Research Forester. First, he conducted research in fire management planning and economics while located at the Forest Fire Lab, Riverside, CA. During 1990 and 1991, while stationed in Madison, WI, at the Forest Products Lab, he collaborated with a research work unit studying atmospheric deposition effects on trees in the western United States. Since 1991, he has been a research scientist, Southeastern Forest Experiment Station, conducting research in primary processing and products of hardwood species. Current responsibilities involve research and development of computer-aided manufacturing systems in the area of primary hardwoods processing and automation. His particular areas of interest are machine vision systems, pattern recognition, automated lumber grading and remanufacturing, and neural networks.

Dr. Schmoldt is an associate editor for *Computers and Electronics in Agriculture*, a contributing editor for *AI Applications*, and the chairperson of the International Union of Forestry Research Organizations working party S4.11-03, Information Management.

Dongping Zhu (M'92) was born in Hunan Province, People's Republic of China, on December 24, 1958. He received the B.S. and M.S. degrees in electronic communications from Dalian University of Technology (formerly Dalian Institute of Technology), Dalian, China, in 1982 and 1985, respectively. He received the M.S. and Ph.D. degrees, both in electrical engineering from Virginia Polytechnic Institute and State University, Blacksburg, in 1989 and 1993.

From 1992 to 1994, he was a Staff Scientist with InVision Technology, Foster City, CA. Since December 1995, he has been a Senior Staff Scientist with Globalstar, San Jose, CA. His research areas include digital signal processing, digital image processing, machine vision, artificial intelligence, and satellite communication system simulations.

Philip A. Araman received the B.S. degree in WOOD Science and Technology from North Carolina State University, Raleigh, in 1968, and the M.S. degree in forest products from Virginia Polytechnic Institute and State University, Blacksburg, in 1975.

Since 1987 he has been a Project Leader/Research Forest Products Technologist, USDA Forest Service, Southeastern Forest Experiment Station, Brooks Forest Products Center, Virginia Polytechnic Institute and State University. He is also a Senior Research Scientist with the Department of Wood Science and Forest Products VPISU and the Director of the Center for Automated Processing of Hardwoods. His research projects have a research mission to increase U.S. competitiveness and share of domestic and foreign markets by developing automated primary hardwood processing technologies, and by developing new or improved products made from low- and medium-grade hardwood sawtimber and nonselect species. Research underway includes: multiple sensor scanning of hardwood products (color carera, laser/camera, x-ray), computer-aided sawmill edging and trimming, computer vision grading of hardwood lumber, internal scanning of hardwood logs, log processing computer training tools, edging and trimming computer training tools, and hardwood processing automation and simulation.

Mr. Araman is a member of the Forest Products Research Society, the Southern Forest Economics Workers, the Hardwood Research Council, and the American Hardwood Export Council.